Pergamon

Int. J. Impact Engng Vol. 18, No. 3, pp. 339–353, 1996

0734–743X(95)00037-2
0734–743X/96 $15.00 + 0.00

A SIMPLE MODEL TO PREDICT RESIDUAL VELOCITIES OF THICK COMPOSITE LAMINATES SUBJECTED TO HIGH VELOCITY IMPACT

C. T. SUN† and S. V. POTTI

School of Aeronautics and Astronautics, Purdue University, West Lafayette, Indiana 47907-1282, U.S.A.

(*Received* 17 *March* 1995; *in revised form* 14 *June* 1995)

Summary—A punch curve was used as the "structural constitutive model" that captures the highly nonlinear behavior of the laminate in the penetration process. This model in conjunction with a special two-noded ring element based on the Mindlin thick plate theory was employed to model damage processes during static and dynamic penetration. Different criteria for initiation of damage and plug formation were investigated, and the damage initiation and progression in the target and its effect on the dynamic response were estimated. The model predicts the residual velocity of the projectile at the end of the penetration process. The predicted residual velocities show good agreement with the experimental residual velocities for a range of striking velocities near and above the ballistic penetration limit velocity of the target

1. INTRODUCTION

The need for high strength, high stiffness and lightweight materials for structural applications has increased the use of fiber reinforced composite laminates. Composites are used in aircraft and land-based vehicles which must be designed to withstand impact at high speeds by broken engine parts, turbine blades and other debris. Many applications involve the survivability of personnel and equipment against impact by projectiles travelling at high speeds. The need for high resistance of these materials against penetration by high velocity projectiles is critical. Thus, it is important to have an understanding of the penetration process of these laminates by a projectile under high velocity impact conditions.

The damage of composite laminates under low velocity impact has been studied extensively [1–5], but relatively little progress has been achieved in understanding penetration of these laminates. Recently, Abrate [5] made a review of research in low velocity and ballistic impact of laminated composite materials. A few experimental studies have measured the residual velocities of various laminates under a range of striking velocities [6–10]. Wu *et al.* [7] used laser doppler anemometry to measure the velocity of a projectile during penetration of 8 ply glass–epoxy laminates. Zhu *et al.* [11] described a phenomenological model for Kevlar-29–polyester laminates penetrated by a conical faced projectile which used a finite difference scheme to capture the assumed local and global deformation modes of the target during penetration. The rate effects were incorporated by the use of a dynamic yield stress value in the model. Goldsmith *et al.* [12] used an approach similar to [8] to predict the energy required for penetration of woven graphite–epoxy laminates by cylindro-conical projectiles. Fiber breakage, hole enlargement and petal bending were assumed to expend the major part of energy during penetration. Dynamic effects of the target were not considered in [12], and the difference between static and dynamic penetration was taken to be caused by the difference in the number of fiber breaks in the two cases.

Lee and Sun [9] proposed a model based on the static punch curve to characterize the penetration process of graphite–epoxy laminates. This model was then used to predict the ballistic limit of laminates and compared with results from dynamic impact tests [10]. Sun and Potti [13] proposed a simple model that gives an upper bound for the residual velocities for the laminates considered in the study. Jenq *et al.* [14] used an approach similar to [10] in

† Author to whom correspondence should be addressed.

using the quasi-static punch curve to determine the major damage modes during penetration by a hemispherically tipped penetrator. This static penetration information was used in a dynamic finite element code to predict the ballistic limits of woven glass–epoxy laminates.

During penetration of composite laminates by impact of projectiles, many complicated phenomena occur: transient local and global deflection of the target under impact and dynamic forces, damage initiation and progression, formation of a plug, push-out of the plug, etc. A detailed modeling of the damage progression during penetration would be a very difficult task. In this study, a new approach has been proposed in which the penetration of a target under quasi-static conditions (the punch curve) was used to derive a "structural constitutive model" that captures the highly nonlinear behavior of the laminate during contact and penetration. The fundamental static punch curve was then used in conjunction with a Mindlin plate model to replicate the penetration through the laminate in the dynamic case. This approach allows one to use a global model such as the plate model to indirectly account for the very complicated failure process in the laminate. This analytical model should be capable of predicting the penetration behavior of various target sizes and for different target thicknesses from information obtained from one static punch curve.

2. EXPERIMENTAL INVESTIGATION

Graphite–epoxy (Hercules AS4-3501/6) laminates 30.5 cm by 30.5 cm were fabricated from which specimens 9 cm by 9 cm were cut to be used for static and dynamic tests. A quasi-isotropic lay-up with the ply sequence of $([0/90/\pm 45]_s)_n$ was chosen for the sake of simplification of the damage mechanisms that are produced. Laminates of 32, 48, and 64 ply thickness (corresponding to $n = 4$, 6, and 8) were selected to study the thickness effect on the penetration process. Static punch-through and dynamic penetration tests were performed on these laminates with indentors and projectiles that have the same shape and rigidity.

2a. *Quasi-static punch experiments*

The static punch-through tests were done for AS4/3501-6 graphite–epoxy laminates of 32, 48 and 64 ply thickness of different specimen sizes. A cylindrical indentor with a flat indenting face 14.61 mm in diameter d was used. The specimens were clamped between two steel plates with circular exposed sections. Specimens with exposed diameters D of 3 times and 5 times the penetrator diameters were studied. The quasi-static punch experiments were performed under displacement control. The displacement of the indentor was measured using an LVDT mounted between the indentor shank and the fixture used to clamp the specimen. Figure 1 shows the configuration of the specimen and the penetrator and the typical damage pattern of shear plug formation after penetration. The six target sizes studied are listed in Table 1.

Typical load–displacement punch curves are shown in Fig. 2. The load increases with displacement of the penetrator until the initiation of damage. The load drops after the first peak with the onset of delamination in the specimen. The load then increases and decreases again in a progressive fashion with the progression of delamination until the plug is formed at

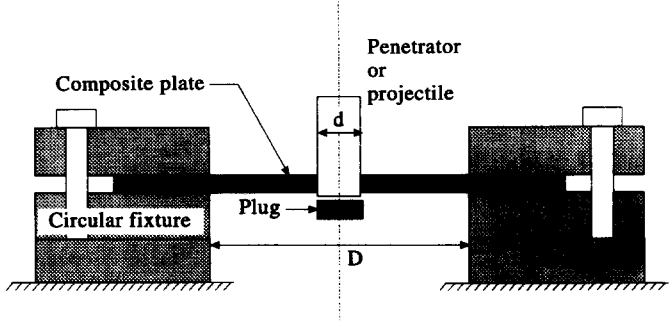

Fig. 1. Typical experimental setup and damage pattern after penetration with the formation of the shear plug.

Table 1. Specimen thickness and sizes used in the experiments
Projectile diameter $d = 14.6$ mm

		Thickness (mm)	*D/d*	*Diameter (mm)*
1	32 ply	4.1	3	43.8
2	32 ply	4.1	5	73.0
3	48 ply	6.5	3	43.8
4	48 ply	6.5	5	73.0
5	64 ply	8.6	3	43.8
6	64 ply	8.6	5	73.0

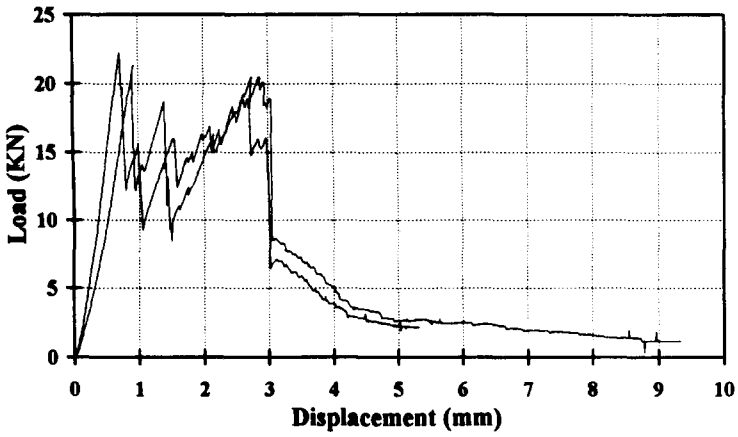

Fig. 2. Typical quasi-static punch curves for a graphite–epoxy laminate (48 ply $D/d = 3$).

a certain load which corresponds to the big drop in the punch force. The plug is then pushed out under a friction force which corresponds to the long tail of the punch curve. It was inferred from the punch curves for different spans that the load at the initiation of damage and the load at final plug formation were approximately the same for the two spans of the same laminate, and the plug formation load was about the same as the load at initiation of damage.

2b. *Dynamic penetration tests*

A high velocity air gun was used to perform dynamic penetration experiments. Compressed nitrogen gas was used to pressurize the gun which was then triggered using a high pressure mechanical release valve. Care was taken to align the gun so that the projectiles impact normally at the center of the specimen. Hardened steel cylinders 14.6 mm in diameter were used as projectiles. The striking face was machined flat. Two types of projectiles were used. Projectile 1 was about 22.9 mm long (mass 30 g), and projectile 2 was about 9.3 mm long (mass 12 g). During impact tests with both projectiles, the impressions of the projectiles on the target were circular in shape with a diameter the same as that of the projectile. No evidence of tumbling of the projectiles before they hit the target was noticed.

The striking velocities were estimated by measuring the time of flight between three photo-emitter/detector units mounted 90 mm apart in the path of the projectile beyond the accelerating barrel portion of the gun. The residual velocities after the projectile exits from the rear of the target were estimated by two methods. In the first method, the time taken between the shattering of two thin glass plates mounted about 115 mm apart in the path of the projectile after penetration of the specimen was measured. A correction based on a calibration curve was applied to the measured residual velocities to obtain the corrected residual velocities. In the second method, the presence of the projectile when it passes through an electromagnetic coil was sensed from the change in flux produced. The time of

flight of the projectile between two such sensing coils mounted about 275 mm apart was measured. These residual velocities measured by the electromagnetic coils were calibrated against incident velocities measured by the photo-emitter/detector units.

3. SIMPLE ENERGY MODELS

3a. *Static punch-through energy model*

The punch curve captures in a quasi-static manner all the damage events that occur during penetration. The energy under the punch curve is the energy dissipated during quasi-static penetration. Preliminary estimations of the residual velocities during dynamic penetration were obtained by subtracting the quasi-static penetration energy from the incident projectile energy. A residual velocity can be calculated for each of the impact tests under various incident velocities assuming that the penetration process is essentially similar to the penetration process in the quasi-static case. Thus, the predicted residual velocity is given by the equation,

$$v_{RS} = \sqrt{v_S^2 - \frac{2}{m} E_{SP}} \tag{1}$$

where v_{RS} is the predicted residual velocity, m is the mass of the projectile, v_S is the striking velocity and E_{SP} is the static penetration energy as calculated above. These estimated values were higher than the experimentally measured residual velocities, as shown in Figs 3–5. This implies that the energy consumed by the target during dynamic penetration was higher than in the quasi-static case even though the modes of failure are similar for the two cases.

3b. *Modified energy model*

The static punch-through energy approach above was modified to obtain more accurate prediction of the residual velocities for the various specimens and projectiles tested in this study. The energy required to complete the dynamic penetration of a target by the projectile may depend on the impact velocity v_S. If we assume that the dynamic penetration energy E_{DP} remains a constant for a range of incident velocities, we can estimate a value for the dynamic penetration energy from the energy balance equation

$$E_{DP} = \tfrac{1}{2} m(v_S^2 - v_R^2) \tag{2}$$

where v_R is the experimentally measured residual velocity at a particular incident velocity v_S

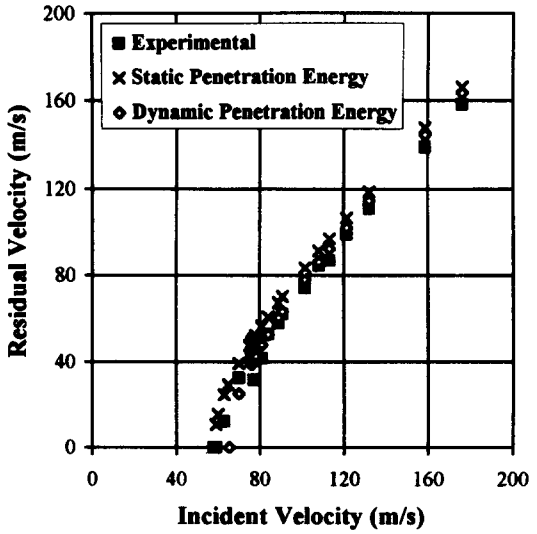

Fig. 3. Residual velocities vs incident velocities for 32 ply $D/d = 3$ laminates by projectile 1.

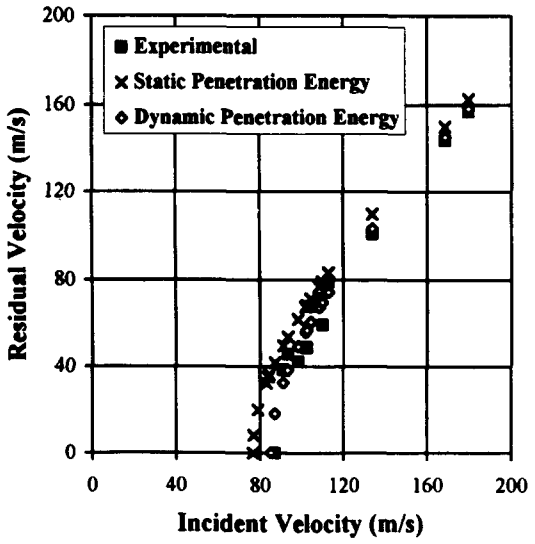

Fig. 4. Residual velocities vs incident velocities for 48 ply $D/d = 3$ laminates by projectile 1.

for the particular specimen and projectile. Using a constant E_{DP} based on the experimental data, the residual velocities can be estimated using Eqn (1) with E_{DP} replacing E_{SP}. Figures 3–6 show that the predictions agree very well with the experimental data. It can be concluded that this method provides a very simple and, at the same time, accurate estimate for residual velocities of the projectile at different incident velocities. This method has the potential of being a very practical design criterion for estimating the penetration characteristics of composite panels in different applications.

The dynamic penetration energy E_{DP} is higher than the static penetration energy E_{SP} at all ranges of incident velocities for all specimens. At impact velocities much higher than the ballistic limit velocities, the kinetic energy of the projectile before and after penetration is very large compared to the dynamic penetration energy E_{DP} of the target, thus minimizing the difference between the residual velocities predicted using the two energy models described above. Further, at higher incident velocities, the dynamic penetration energy of the smaller ($D/d = 3$) and larger ($D/d = 5$) specimens of the same thickness remain almost the same. This indicates that at high incident velocities, the dynamics and damage in the larger specimen are

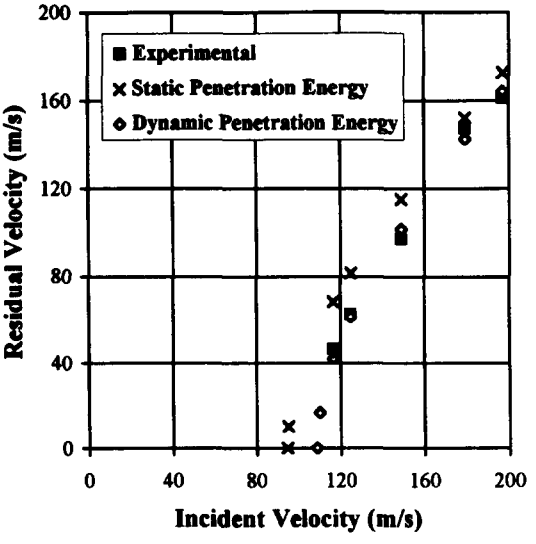

Fig. 5. Residual velocities vs incident velocities for 64 ply $D/d = 3$ laminates by projectile 1.

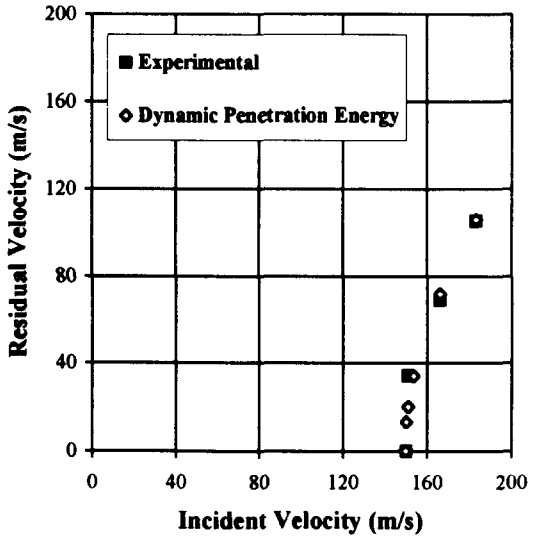

Fig. 6. Residual velocities vs incident velocities for 48 ply $D/d = 5$ laminates by projectile 2.

similar to those in the smaller specimen, showing that localization of the penetration process may be occurring at high impact velocities.

4. THE SIMPLE RING MODEL

The modified energy approach described above requires data from a few dynamic penetration tests to provide a good estimate of the dynamic penetration energy E_{DP}. These dynamic penetration tests must be performed for each projectile–target combination to estimate the value of E_{DP} for that combination. It is also unclear if the value of the dynamic penetration energy will remain a constant for a larger range of incident velocities. Thus, it is necessary to model the dynamic response of the target in order to accurately estimate the energy consumed during dynamic penetration. A dynamic model would also provide insight into the various damage mechanisms that occur during the penetration process. This model should be able to predict the dynamic response of the targets of different sizes during penetration by different types of projectiles and at different ranges of incident velocities, without performing any dynamic penetration tests. For this purpose, a ring element was formulated to model the static and dynamic response of the target plate. Mindlin plate theory was used to capture the bending behavior of thick plates. The element is based on the finite element discretization of a circular plate under axisymmetric loading. This element has 2 nodes along the centerline of the plate with 2 degrees of freedom, transverse deflection and rotation, per node as shown in Fig. 7.

The shape functions were chosen to capture the deflection of a circular plate with transverse shear deformation in an exact fashion for the loading shown in Fig. 8. The displacement w and rotation ϕ were assumed to be of the form

$$w(r) = a_1 r^2 + a_2 \ln(r) + a_3 r^2 \ln(r) + a_4 \tag{3}$$

$$\phi(r) = b_1 r + b_2 r \ln(r) + \frac{b_3}{r}. \tag{4}$$

In terms of the coordinates, displacements and rotations at the nodes of the element, the displacement and rotation functions were derived as

$$w = f_1(r)w_1 + f_2(r)\phi_1 + f_3(r)w_2 + f_4(r)\phi_2 \tag{5}$$

$$\phi = p_1(r)w_1 + p_2(r)\phi_1 + p_3(r)w_2 + p_4(r)\phi_2 \tag{6}$$

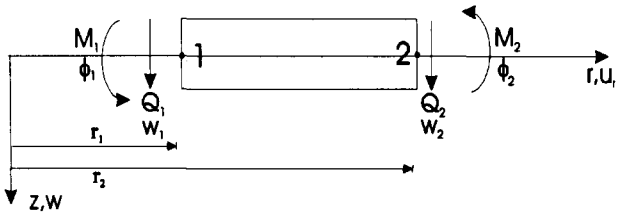

Fig. 7. The ring element with nodal degrees of freedom and generalized nodal forces.

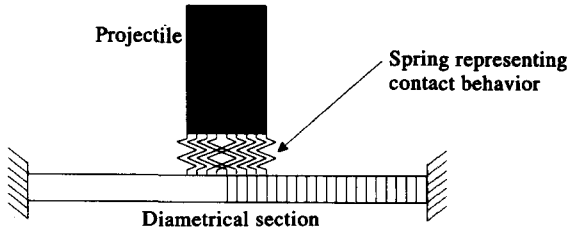

Fig. 8. Discretization of the specimen into ring elements and compression elements.

where f_i and p_i are given in the Appendix. The 4 × 4 stiffness matrix was obtained as

$$\begin{Bmatrix} Q_1 \\ M_1 \\ Q_2 \\ M_2 \end{Bmatrix} = \begin{bmatrix} K_{11} & K_{12} & K_{13} & K_{14} \\ K_{21} & K_{22} & K_{23} & K_{24} \\ K_{31} & K_{32} & K_{33} & K_{34} \\ K_{41} & K_{42} & K_{43} & K_{44} \end{bmatrix} \begin{Bmatrix} w_1 \\ \phi_1 \\ w_2 \\ \phi_1 \end{Bmatrix} \tag{7}$$

where for example, the term K_{11} is obtained as

$$K_{11} = 16\pi \Big/ \left(\frac{1}{\bar{D}} \left\{ (r_2^2 - r_1^2) - \frac{4r_1^2 r_2^2}{(r_2^2 - r_1^2)} \ln \left(\frac{r_2}{r_1} \right)^2 + \frac{1}{\bar{G}} \ln \left(\frac{r_2}{r_1} \right) \right) \right. \tag{8}$$

In Eqn (8)

$$\bar{D} = \frac{\bar{E}_{rr} h^3}{12(1 - \nu_r^2)} \tag{9}$$

is the bending stiffness, and

$$\bar{G} = \kappa \bar{G}_{rz} h \tag{10}$$

is the transverse shear rigidity, h is the thickness of the specimen and κ is the shear correction factor taken here as 5/6.

This element can be used to perform an axisymmetric analysis of penetration under static and impact loading. The circular specimen was then discretized using these elements to perform an axisymmetric analysis. In this model, the indentor was discretized as a single node. The contact between the indentor and the specimen is modeled using contact springs between the single node representing the indentor and the elements in the specimen which overlap in diameter with the indentor; see Fig. 8. The contact element stiffness k_i at a node i of the specimen is taken proportional to the part of the area A_i of the elements it represents as

$$k_i = \frac{\bar{E}_{zz} A_i}{L} \tag{11}$$

where L is the length of the contact spring. The contact element between the projectile and the ring element was assumed to extend from the top until the midplane of the plate. The homogenization scheme of Sun and Li [15] for thick laminates was used to calculate the value of the effective modulus $\bar{E}_{zz}$ for the laminate.

5. MODELING OF THE QUASI-STATIC PUNCH CURVE

Lee and Sun [9] modeled the quasi-static penetration curves of 16 and 32 ply graphite–epoxy laminates using effective elastic properties which were degraded to simulate the reduced load carrying capability of the laminate after the onset of delaminations. In this study, a simulation of the displacement controlled quasi-static penetration test was performed. The load–displacement curves for the various laminates and different specimen spans obtained from the static punch experiments were reproduced using the model in these simulations.

The initial undamaged portions of the load–displacement curves were modeled using the elastic properties of the laminate. Since the deformation of the quasi-isotropic circular laminate specimens was assumed to be axisymmetric, effective moduli $\bar{E}_{rr}$ and $\bar{G}_{rz}$ of the laminates were used. The ply properties for graphite–epoxy (AS4/3501-6) used in this study are listed in Table 2. The effective modulus scheme of Sun and Li [15] for thick composite laminates was used to calculate the average elastic constants for the repeating sublaminate of $[0/90/\pm 45]_{s,n}$. The average effective laminate elastic properties for the quasi-isotropic lay-up of $[0/90/\pm 45]_{s,n}$ used in this study are listed in Table 3.

A typical example of the experimental and simulated curves is shown in Fig. 9 (for 32 ply $D/d = 3$ specimens). The displacement for the initial undamaged region obtained using the model underpredicts the experimentally measured values. The displacement plotted in the load–displacement curves obtained from the model is a sum of local indentation and plate deflection. The experimental indentation will have some local, nonlinear and inelastic components that are not captured using the ring and contact element model. This difference will not significantly affect the subsequent penetration process in the static and dynamic cases.

5a. *Damage modeling during static penetration*

Modeling of the quasi-static force–displacement curve was guided by the requirement that the simulated curve should provide the same strain energy expended in producing damage and plug formation as the average of the experimental curves.

In this study, the modeling of the damaged material was attempted in a global sense to reproduce the load–displacement curve during quasi-static penetration since a detailed

Table 2. Material properties for graphite–epoxy (AS4-3501-6)

E_1	138.0 GPa
E_2	9.65 GPa
E_3	9.65 GPa
G_{23}	3.24 GPa
G_{13}	5.24 GPa
G_{12}	5.24 GPa
ν_{23}	0.49
ν_{13}	0.3
ν_{12}	0.3
ρ	1550 kg/m^3

Table 3. Effective properties for the $[0/90/\pm 45]_{s,n}$ laminates

$\bar{E}_x$	53.7 GPa
$\bar{E}_y$	53.7 GPa
$\bar{E}_z$	11.7 GPa
$\bar{G}_{yz}$	4.0 GPa
$\bar{G}_{xz}$	4.0 GPa
$\bar{G}_{xy}$	20.7 GPa
$\bar{\nu}_{yz}$	0.33
$\bar{\nu}_{xz}$	0.31
$\bar{\nu}_{xy}$	0.31

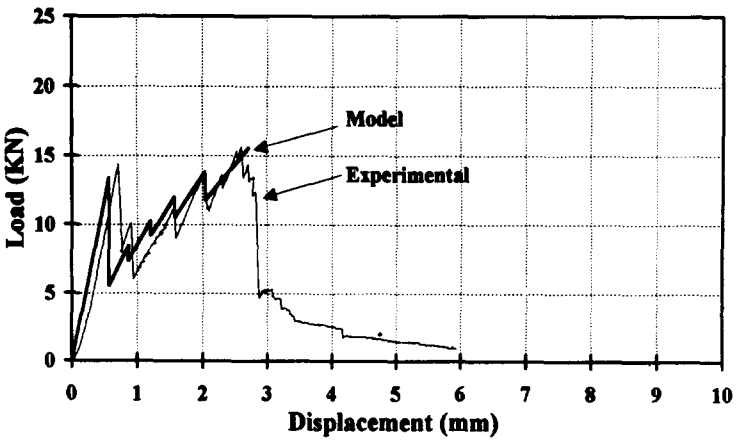

Fig. 9. Static punch curves for 32 ply $D/d = 3$ specimens showing experimental and simulated curves.

modeling of the delaminated plate is very difficult and impractical. Since the major damage to the material before plug formation consists of matrix cracks and delaminations, the global modeling of damage was achieved by reducing the effective shear modulus $\bar{G}_{rz}$ of the laminate to a degraded value $\bar{G}^*_{rz}$. The effective in-plane modulus $\bar{E}_{rr}$ was assumed to remain the same as the undamaged value since there is no major fiber breakage in the material until the plug is formed. X-radiography of the specimens after initiation of damage showed that the superposition through the thickness of delaminations extends from the center to the clamped boundary of the specimen although the delamination may not extend throughout the span at any interface. Lee and Sun [9] showed that the density of delaminations in the specimen increased with the progression of damage when the specimen was loaded beyond the onset of delamination. This was found to be the case for all the specimens tested in this study. The effective shear modulus was degraded uniformly from the center to the boundary of the specimen to model the damage.

The slope of the damaged region of the experimental load–displacement curve was approximated by choosing the degraded value of the shear modulus $\bar{G}^*_{rz}$. The experimental load–displacement curve after damage initiation was found to show progressive damage behavior with increase of delaminations with increasing penetrator displacement. The load–displacement behavior after initiation of damage until plug formation cannot be modeled using a single value for the degraded shear modulus. A progressive reduction of the effective shear modulus in multiple steps was used to capture the average slope of the load–displacement curve after damage initiation until plug formation.

During the displacement-controlled quasi-static penetration test, damage was initiated in the experiments at a critical damage initiation load. A drop in the penetration force occurs between point A and point B when damage is initiated in the specimen as shown schematically in Fig. 10. The load then increases in a jagged fashion with further displacement of the penetrator until plug formation. For this region, the average of the force–displacement curves of many static penetration tests can be represented by a straight line between points B and C. To reproduce the load–displacement curve using the model, the transverse shear modulus has to be reduced to reach point B from point A. The shear modulus required to reproduce the deflection at point C is lower than that required to reach point B because of the additional damage produced in the laminate from B to C. Thus, the region from B to C cannot be modeled in one step. The modeling of the force–displacement curve from B to C was done using a piecewise linear–elastic approach. The load level between point B and point C was divided into five load steps. For each of these load steps, a value of the reduced shear modulus was determined that would give a close approximation to the average slope of the load–displacement curve between points B and C. At each reduction of transverse shear modulus, the total indentor displacement was taken to remain constant to simulate the displacement controlled test. When each region of progressive damage is initiated, the load drops because of the reduction of transverse shear rigidity. This amount of load drop was

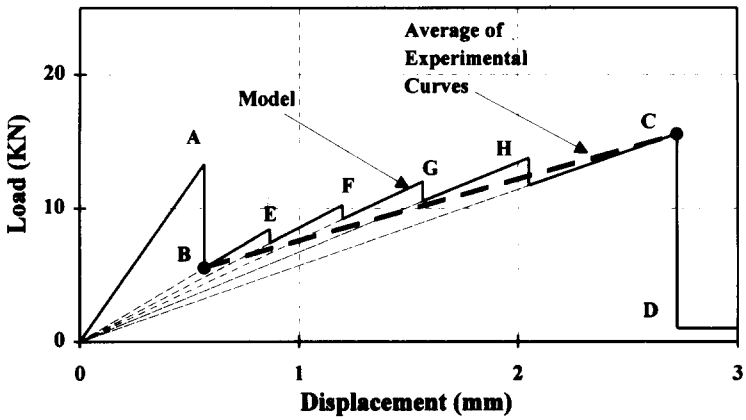

Fig. 10. Schematic of a static punch curve showing experimental and simulated curves.

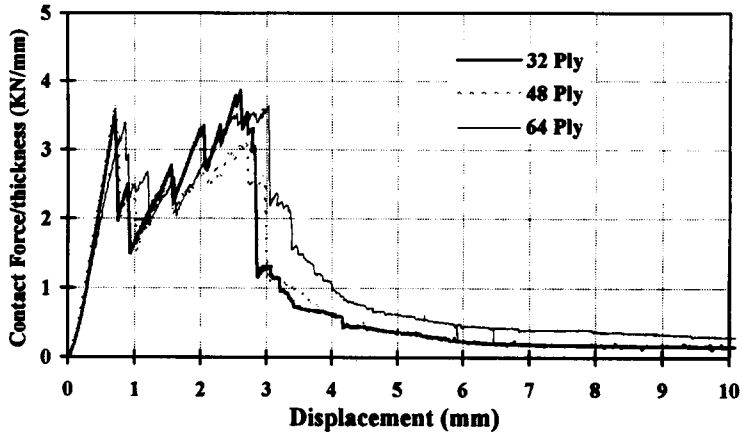

Fig. 11. Normalized experimental punch curves for the different specimens.

determined by using the ring element with the reduced shear rigidity. The plug was assumed to form when the load at point C was reached and the quasi-static simulation was stopped.

5b. *Normalized punch curves*

The contact forces of the punch curves for different specimens were normalized with the thickness of the specimen. Figure 11 shows the normalized curves for the $D/d = 3$ specimens of different thicknesses. This figure indicates that in the form, the punch curves for specimens of different thicknesses would collapse into a single curve. This master curve can be used to recover the punch curve for the specimen of any given thickness. Thus, the static penetration test needs to be performed for only one specimen of the same D/d ratio. The information obtained from this one test will be shown to be sufficient to predict the dynamic penetration of specimens of all sizes.

6. MODELING OF DYNAMIC IMPACT AND PENETRATION

The dynamic impact behavior at different striking velocities was modeled. The model consists of 330 elements. The node in the model which represents the projectile was given an initial velocity v_S equal to the striking velocity of the projectile. The equations of motion were then solved at each time step using the Newmark-Beta numerical procedure. Lumped mass and rotational inertia matrices were used. The linearized system of algebraic equations were solved at each time step using an IMSL solver with iterative refinement. At the end of each time step, the displacements, velocities and accelerations of each node, the contact force, the

contact pressure distribution, and the shear forces at various locations of the laminate specimen were recorded. At plug formation, the velocity of the projectile was recorded. The energy for push-out of the plug was then subtracted from the remaining kinetic energy of the projectile after plug formation, and the residual velocity of the projectile was calculated. The energy needed for plug push-out during dynamic penetration is assumed to remain the same as in the quasi-static penetration case which was calculated by integrating the force–displacement curve after plug formation and adding the energy required for the projectile push-out at a constant frictional force.

6a. *Criteria for damage and penetration*

Different criteria to trigger damage initiation, progression and plug formation were investigated. Contact force, shear force or shear strain at the contact periphery, and plate deflection could be used as failure criteria. Damage initiation, progression and plug formation were taken to be triggered during dynamic penetration when the values of the parameter used as the criterion reached the critical values obtained from the quasi-static punch curves. The simulation takes about 15 min to complete on a Sun-Sparc20 workstation.

Using contact force as the criterion predicted early damage initiation and plug formation and hence higher residual velocities than experimental values. The contact force is much larger in the dynamic impact case than that in the static case because of the inertia effect of the target. Lee and Sun [10] also found the contact force to be highly oscillatory and unsuitable as a failure criterion.

The plate shear strain at the contact periphery was shown to be a parameter that can be used to predict the quasi-static penetration of different specimens. When the plate shear strain at the periphery of contact was used as the critical parameter that controls damage initiation, progression and plug formation in the case of dynamic impact, the predicted residual velocities at low incident velocities were in good agreement with the experimental values. At higher velocities, however, the criterion predicted the occurrence of damage initiation and plug formation a few microseconds after impact. This was due to the rapid increase of contact stresses and shear strains in the region at the periphery of contact while the stress waves were still propagating towards the boundary of the specimen. This prediction of premature failure makes the use of this parameter to predict dynamic penetration questionable.

Deflection of the central region of the plate can be used as a global parameter for triggering damage in the plate. For the $D/d = 3$ specimens, we used the deflection between the periphery of the penetrator and the clamped edge. The critical values of plate deflection at which delamination initiation and plug formation occur are obtained from the static punch curve. For the $D/d = 5$ size specimens, we used the differential deflection between the periphery of the penetrator and the location of a diameter $D = 3d$ corresponding to the boundary of the smaller specimen. For the larger specimens, the differential deflection as defined above, rather than the total deflection of the specimen, was used as the criterion for damage initiation and plug formation based on the punch curve for the specimen $D/d = 3$. This procedure was adopted based on the assumption that, in dynamic impact, the response of the region $r \leqslant 3d$ in the $D/d = 5$ plate is basically the same as that of the $D/d = 3$ plate.

Figure 12 shows the dynamic deflection profile of the midplane of a $D/d = 3$ specimen at the instants of damage initiation and plug formation. Figure 13 shows the deflection profiles for a larger specimen ($D/d = 5$) under similar impact conditions. The deflection at the edges of the specimen have a small amplitude due to the clamped nature of the boundary. The deflection profiles of the central region of the plate which control the initiation of damage and plug formation are very similar in both cases. It appears that the reflection of elastic waves from the boundary does not seem to significantly affect the deflection of the central region of the target. Outgoing stress waves produced by projectile contact with the target dominate the dynamic deflection. This effect is accentuated at higher impact velocities. The penetration process in targets with large diameters can be expected to be similar to that in smaller targets.

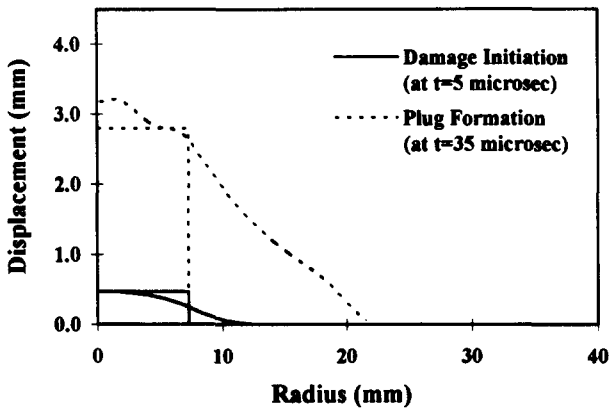

Fig. 12. Dynamic deflection profiles for 48 ply $D/d = 3$ laminates ($v_S = 100$ m/s, projectile 1).

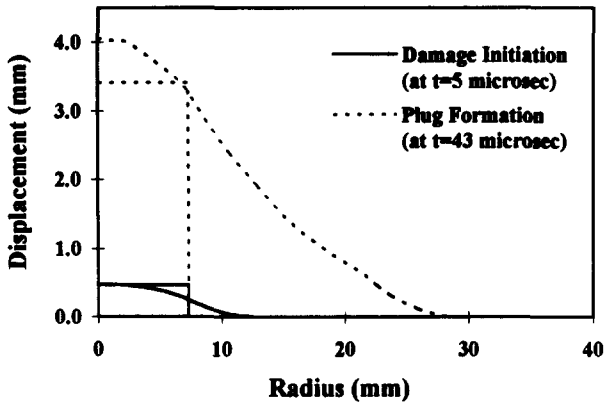

Fig. 13. Dynamic deflection profiles for 48 ply $D/d = 5$ laminates ($v_S = 100$ m/s, projectile 1).

6b. *Results of the simulation of dynamic penetration*

Plate deflection serves as the global criterion for damage initiation and predicts residual velocities that compare well with experimental residual velocities. Figures 14–17 show the relation between residual and striking velocities using displacement (or differential displacement) as the damage initiation criterion for different specimens. It can be seen that using displacement as the failure criterion provides very good predictions of residual velocities for different specimens and projectiles based on the data from static punch test of the $D/d = 3$ specimen.

7. CONCLUSIONS

For graphite–epoxy targets of different thicknesses and sizes evaluated in this study, residual velocities predicted using the dynamic energy model compare very well with experimental data for a large range of incident velocities. Ballistic limits are also predicted with sufficient accuracy. The dynamic response model can be used along with the critical deflection criterion to predict high-speed impact and penetration of composite laminate targets of various thicknesses and sizes based on the information obtained from a single static punch-through test.

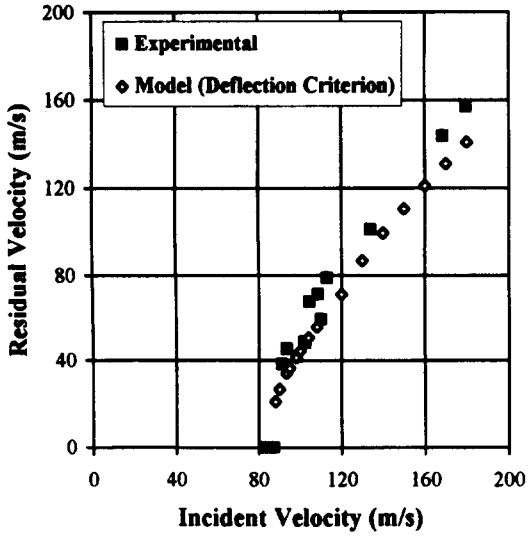

Fig. 14. Residual velocities vs incident velocities for 48 ply $D/d = 3$ laminates by projectile 1.

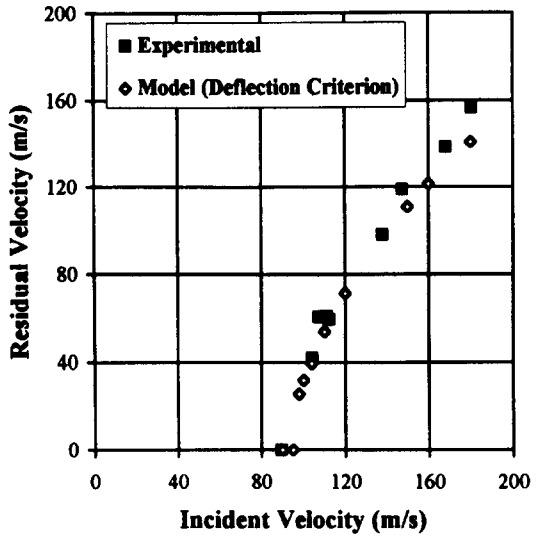

Fig. 15. Residual velocities vs incident velocities for 48 ply $D/d = 5$ laminates by projectile 1.

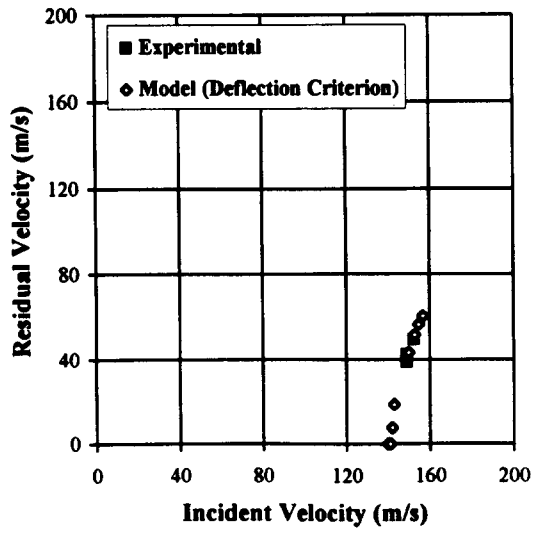

Fig. 16. Residual velocities vs incident velocities for 48 ply $D/d = 3$ laminates by projectile 2.

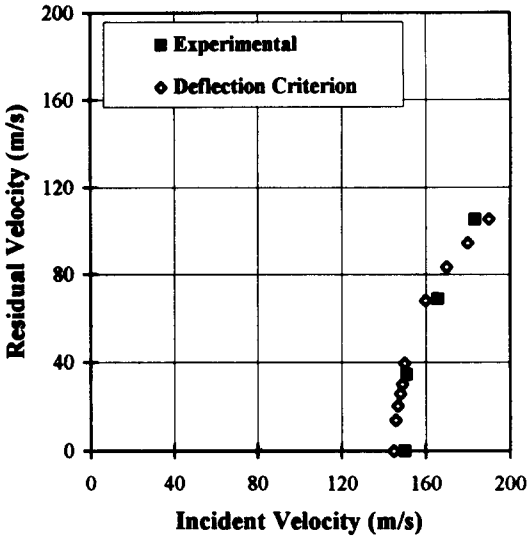

Fig. 17. Residual velocities vs incident velocities for 48 ply $D/d = 5$ laminates by projectile 2.

Acknowledgement—This work was supported by the U.S. Army Research Office under Grant DAAL03-91-G-0013 to Purdue University. Dr K. Iyer was the grant monitor.

REFERENCES

1. N. Cristescu, L. E. Malvern and R. L. Sierakowski, Failure mechanisms in composite plates impacted by blunt-ended penetrators. *Foreign Object Impact Damage to Composites*, ASTM STP 568, pp. 159–172 (1975).
2. S. P. Joshi and C. T. Sun, Impact induced fracture in a laminated composite, *J. Comp. Mat.* **19**, 51–66 (1985).
3. K. N. Sivakumar, W. Elber and W. Illg, Prediction of impact force and duration due to low-velocity impact on circular composite laminates. *J. Appl. Mech.* **52**, 674–680 (1985).
4. W. J. Cantwell and J. Morton, Impact perforation of carbon fibre reinforced plastic. *Comp. Sci. Tech.* **38**, 119–141 (1990).
5. S. Abrate, Impact on laminated composite materials. *Appl. Mech. Rev.* **47**, 517–544 (1994).
6. S. J. Bless and D. R. Hartman, Ballistic penetration of S-2 glass laminates. *Proc. 21st Int. SAMPE Conf.* Vol. 21, pp. 852–866 (1989).
7. E. Wu, C.-Z. Tsai and Y.-C. Chen, Penetration into glass/epoxy composite laminates. *J. Comp. Mat.* **28**, 1783–1802 (1994).
8. G. Zhu, W. Goldsmith and C. K. H. Dharan, Penetration of laminated kevlar by projectiles—I. Experimental investigation, *Int. J. Solids Struct.* **29**, 421–436 (1992).
9. S.-W. R. Lee and C. T. Sun, A quasi-static penetration model for composite laminates. *J. Comp. Mat.* **27**, 251–271 (1993).
10. S.-W. R. Lee and C. T. Sun, Dynamic penetration of graphite/epoxy laminates impacted by a blunt-ended projectile. *Comp. Sci. Tech.* **49**, 369–380 (1993).
11. G. Zhu, W. Goldsmith and C. K. H. Dharan, Penetration of laminated kevlar by projectiles—II. Analytical model. *Int. J. Solids Struct.* **29**, 421–436 (1992).
12. W. Goldsmith, C. K. H. Dharan and H. Chang, Quasi-static and ballistic perforation of carbon fiber laminates. *Int. J. Solids Struct.* **32**, 89–103 (1995).
13. C. T. Sun and S. V. Potti, High velocity impact and penetration of composite laminates. *Proc. ICCM-9, Ninth Int. Conf. Comp. Mat.* Vol. 4, pp. 157–165 (1993).
14. S. T. Jenq, H.-S. Jing and C. Chung, Predicting the ballistic limit for plain woven glass/epoxy composite laminate. *Int. J. Impact Engng* **15**, 451–464 (1994).
15. C. T. Sun and S. Li, Three-dimensional effective elastic constants for thick laminates. *J. Com. Mat.* **22**, 629–639 (1988).

APPENDIX

$$f_1(r) = (f_{11} + f_{12}r^2 + f_{13}\ln r + f_{14}r^2\ln r)/g$$
$$f_2(r) = r_1(f_{21} + f_{22}r^2 + f_{23}\ln r + f_{24}r^2\ln r)/g$$
$$f_3(r) = (f_{31} + f_{32}r^2 + f_{33}\ln r + f_{34}r^2\ln r)/g$$
$$f_4(r) = r_2(f_{41} + f_{42}r^2 + f_{43}\ln r + f_{44}r^2\ln r)/g$$
$$p_1(r) = 4(p_{11}/r + p_{12}r + p_{13}r\ln r)/g$$
$$p_2(r) = r_1(p_{21}/r + p_{22}r + p_{23}r\ln r)/g$$

$p_3(r) = 4(p_{31}/r + p_{32}r + p_{33}r\ln r)/g$

$p_4(r) = r_2(p_{41}/r + p_{42}r + p_{43}r\ln r)/g$

where

$$g = (r_2^2 - r_1^2)\left\{r_2^2 - r_1^2 - 8\frac{\bar{D}}{\bar{G}}\ln\frac{r_2}{r_1}\right\} - 4r_1^2r_2^2(\ln r_1 + \ln r_2)^2$$

$$f_{11} = (r_2^2 - r_1^2)\left\{r_2^2 + 8\frac{\bar{D}}{\bar{G}}\ln r_2\right\} + 2r_1^2r_2^2(\ln r_2 - \ln r_1)(1 - 2\ln r_2)$$

$$f_{12} = -(r_2^2 - r_1^2) - 2(r_2^2\ln r_2 - r_1^2\ln r_1)$$

$$f_{13} = 2r_1^2r_2^2(r_2^2\ln r_2 - r_1^2\ln r_1) - 8\frac{\bar{D}}{\bar{G}}(r_2^2 - r_1^2)$$

$$f_{14} = 2(r_2^2 - r_1^2)$$

$$f_{21} = r_2^2\{(r_2^2 - r_1^2)\ln r_1 - 2r_1^2\ln r_2(\ln r_2 - \ln r_1)\} + 4\frac{\bar{D}}{\bar{G}}\{r_2^2\ln r_1 - r_1^2\ln r_2\}$$

$$f_{22} = \left\{2r_2^2\ln r_2 - 4\frac{\bar{D}}{\bar{G}}\right\}(\ln r_2 - \ln r_1) + (r_2^2 - r_1^2)\ln r_1$$

$$f_{23} = 2r_1^2r_2^2(\ln r_2 - \ln r_1) - \left\{r_2^2 + 4\frac{\bar{D}}{\bar{G}}\right\}(r_2^2 - r_1^2)$$

$$f_{24} = r_2^2 - r_1^2 - 2r_2^2(\ln r_2 - \ln r_1)$$

$$f_{31} = -(r_2^2 - r_1^2)\left\{r_1^2 + 8\frac{\bar{D}}{\bar{G}}\ln r_1\right\} - 2r_1^2r_2^2(\ln r_2 - \ln r_1)(1 - 2\ln r_1)$$

$$f_{32} = -f_{12};\ f_{33} = -f_{13};\ f_{34} = -f_{14}$$

$$f_{41} = r_1^2\{(r_2^2 - r_1^2)\ln r_2 - 2r_2^2\ln r_1(\ln r_2 - \ln r_1)\} + 4\frac{\bar{D}}{\bar{G}}(r_2^2\ln r_1 - r_1^2\ln r_2)$$

$$f_{42} = \left\{2r_1^2\ln r_1 + 4\frac{\bar{D}}{\bar{G}}\right\}(\ln r_2 - \ln r_1) - (r_2^2 - r_1^2)\ln r_2$$

$$f_{43} = -2r_1^2r_2^2(\ln r_2 - \ln r_1) + \left\{r_1^2 + 4\frac{\bar{D}}{\bar{G}}\right\}(r_2^2 - r_1^2)$$

$$f_{44} = -(r_2^2 - r_1^2) + 2r_1^2(\ln r_2 - \ln r_1)$$

$$p_{11} = -r_1^2r_2^2(\ln r_2 - \ln r_1)$$

$$p_{12} = r_2^2\ln r_2 - r_1^2\ln r_1$$

$$p_{13} = -(r_2^2 - r_1^2)$$

$$p_{21} = r_2^2(r_2^2 - r_1^2) - 2r_1^2r_2^2(\ln r_2 - \ln r_1) + 8\frac{\bar{D}}{\bar{G}}r_2^2(\ln r_2 - \ln r_1)$$

$$p_{22} = -(r_2^2 - r_1^2) + 2(r_2^2\ln r_2 - r_1^2\ln r_1) - \left\{4r_2^2\ln r_2 + 8\frac{\bar{D}}{\bar{G}}\right\}(\ln r_2 - \ln r_1)$$

$$p_{23} = -2(r_2^2 - r_1^2) + 4r_2^2(\ln r_2 - \ln r_1)$$

$$p_{31} = -p_{11};\ p_{32} = -p_{12};\ p_{33} = -p_{13}$$

$$p_{41} = r_1^2(r_2^2 - r_1^2) - 2r_1^2r_2^2(\ln r_2 - \ln r_1) + 8\frac{\bar{D}}{\bar{G}}r_2^2(\ln r_2 - \ln r_1)$$

$$p_{42} = -(r_2^2 - r_2^2) + 2(r_2^2\ln r_2 - r_1^2\ln r_1) - \left\{4r_1^2\ln r_1 + 8\frac{\bar{D}}{\bar{G}}\right\}(\ln r_2 - \ln r_1)$$

$$p_{43} = -2(r_2^2 - r_1^2) + 4r_1^2(\ln r_2 - \ln r_1)$$